K-Star Rapid Rotators and the Detection of Relatively Young Multiple K-Star Systems

by

Matthew Albert Henry Joss

Submitted to the Department of Physics
in partial fulfillment of the requirements for the degree of

Bachelor of Science in Physics

at the

MASSACHUSETTS INSTITUTE OF TECHNOLOGY

June 2014

Author ..... Signature redacted .....
Department of Physics
May 27, 2014

Certified by ..... Signature redacted .....
Saul Rappaport
Professor Emeritus
Thesis Supervisor

Accepted by ..... Signature redacted .....
Professor Nergis Mavalvala
Senior Thesis Coordinator, Department of Physics

K-Star Rapid Rotators and the Detection of Relatively Young Multiple K-Star Systems

by

Matthew Albert Henry Joss

Submitted to the Department of Earth, Atmospheric, and Planetary Sciences
in partial fulfillment of the requirements for the degree of

Bachelor of Science in Earth, Atmospheric, and Planetary Science

at the

MASSACHUSETTS INSTITUTE OF TECHNOLOGY

June 2014

Author .... Signature redacted .....
Department of Earth, Atmospheric, and Planetary Sciences
May 27, 2014

Certified by..... Signature redacted .....
Saul Rappaport
Professor Emeritus
Thesis Supervisor

Accepted by..... Signature redacted .....
Professor Richard P. Binzel
Chairman of the EAPS Undergraduate Committee

K-Star Rapid Rotators and the Detection of Relatively Young Multiple K-Star Systems

by

Matthew Albert Henry Joss

Submitted to the Department of Physics
on May 27, 2014, in partial fulfillment of the
requirements for the degree of
Bachelor of Science in Physics

Abstract

In this thesis, I searched through the *Kepler* light curves of 14,440 K-star targets for evidence of periodicities that indicate rapid stellar rotation. Many Kepler M, K, and G stars show modulations in flux due to rotating star spots, and these have been previously investigated by a number of different groups. Rotational periodicities mediated by the rotation of stellar spots were identified using Fourier transforms of *Kepler* light curves. Additional analytical techniques including the folding of light curves and the utilization of 'sonograms' were used to support our hypothesis that these periodicities arise from the rotation of stellar spots as opposed to planetary transits, binary eclipses, or stellar pulsations. In total, 293 of the Kepler K-star targets exhibited rotational periods, $P_{\rm rot}$, of 2 days or less. Of these 293 targets, 17 systems show two or more independent short periods within the same photometric aperture. Images from the United Kingdom Infra Red Telescope (UKIRT) provide evidence for my conclusion that these 17 targets with multiple periods are likely to be relatively young binary and triple K-star systems. The $\sim 2\%$ occurrence rate of rapid rotation among the 14,440 K star targets is consistent with spin evolution models that presume an initial contraction phase followed by spin down due to magnetic braking where typical K stars would be expected to spend up to a few hundred million years before slowing down to a rotation period of more than 2 days.

Thesis Supervisor: Saul Rappaport
Title: Professor Emeritus

Acknowledgments

I would like to acknowledge Roberto Sanchis Ojeda for providing a code that filters through the Kepler data base and that provides Fourier transforms of specified light curves. His code not only separated the K stars out from the rest of the data, it also performed the renormalization process described in the 'Search for Rapidly Rotating K Stars' section of this thesis. Furthermore I would like to acknowledge Arthur Delarue for writing a code that finds significant periods within a Fourier transform as well as periods that have significant higher order harmonics. I would also like to thank Al Levine for informative discussions as well as for programming advice. I would like to thank Professor Rappaport for his endless support and invaluable help with my research. I would like to thank the Kepler team for providing vast amounts of valuable data to the astrophysical community. Last, I would like to thank my friends and family for providing me with tireless support and for encouraging my studies.

Contents

List of Figures

List of Tables

Chapter 1

Introduction

1.1 K Stars

Stars come in all sorts of varieties, large and small, hot and cool. These various kinds of stars have been categorized into numerous classes. According to the Morgan-Keenan (1943) classification of main sequence stars, the varieties include M, K, G, F, A, B, and O, with O stars being the largest, hottest, and most luminous, and M dwarfs being the smallest and coolest. In this spectrum of stellar classes, our own Sun is classified as a G star. The K stellar class rests just in between the G stars (like our Sun) and M dwarfs: namely K dwarfs are generally about 0.6-0.9 times as massive as our Sun, and they have an effective temperature of about 3850-5250 K. Furthermore, stars fall under one of five luminosity classes (I, II, III, IV, and V) where V class stars are the smallest (dwarfs) and I class stars are the most evolved and the largest stars (supergiants). Figure 1-1 shows where in a Hertzsprung–Russell diagram these stellar luminosity classes lie. I will be focusing my attention on the main sequence (luminosity class V) K dwarf stars in this thesis.

K stars are very interesting targets in the search for extra-terrestrial life because they are about 3 to 4 times more numerous than sun-like stars, and they also can remain on the main sequence for nearly the current age of the Galaxy. Since K stars are smaller and cooler than G stars, it is easily demonstrated that the habitable zone around such a K star would be closer in to the host star than around a G star. The

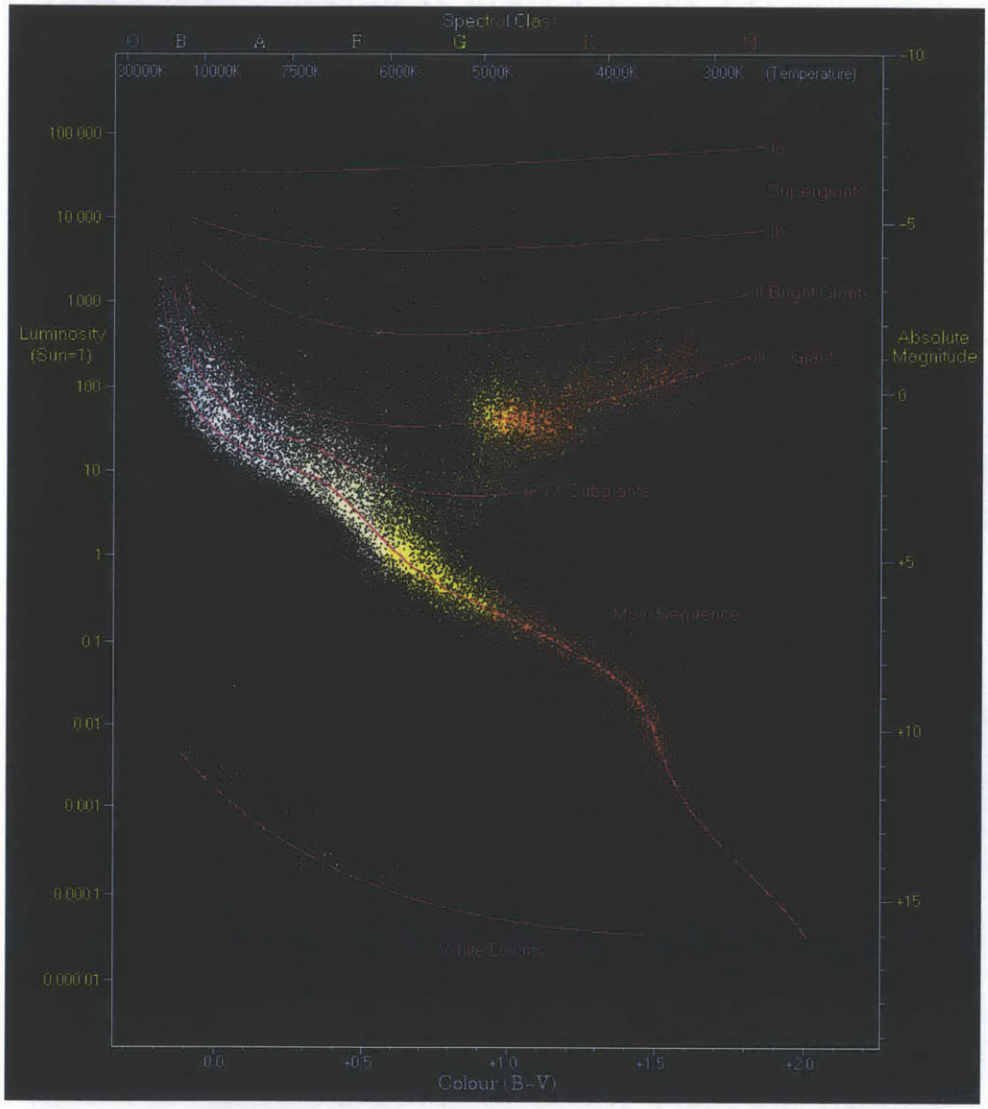

Figure 1-1 An illustration of the different stellar luminosity classes superposed on a Hertzsprung–Russell diagram. In this paper, I will be focusing on the main sequence (luminosity class V) K dwarf stars. Image source: http://www.atlasoftheuniverse.com/hr.html

average surface temperature of a terrestrial planet with no atmosphere, an albedo α, and a distance a from its host star (assuming a circular orbit) is given by:

$$T_{\rm eq} = T_{\rm star}\sqrt{\frac{R_{\rm star}}{2a}}(1-\alpha)^{\frac{1}{4}} \tag{1.1}$$

where $T_{\rm star}$ is the effective temperature of the star and $R_{\rm star}$ is the radius of the star. This equation is derivable by assuming that the star is radiating a constant amount of power, the planet is in a circular orbit about its host star and has no atmosphere, and the planet is in radiative equilibrium with its surroundings. By examining this formula, one can readily understand how, by decreasing the temperature of the star, $T_{\rm star}$, an orbiting planet would consequentially need to have a smaller orbital distance (a) in order for the planet to remain in the habitable zone. Furthermore, habitable planets around K stars are easier to detect via the transit method than habitable planets around G stars because the likelihood that a planet will transit its host star increases as the orbital distance of the star decreases, with the transit probability given by $R_{\rm star}/a$. Also, the transit depth equals $(R_{\rm planet}/R_{\rm star})^2$, so a smaller stellar radius increases the transit depth. These facts make K stars an excellent class to observe in the search for habitable exoplanets. Clearly it is important to study and to understand K stars and the photometric light variations that they can produce for the purpose of finding and categorizing more habitable planets.

At the beginning of the life of a K star, a cloud of gas and dust gravitationally contracts[1] forming a group of stars that are rapidly rotating (e.g., Klessen 2011, Baraffe et al. 2002). Once these young stars contract to near the main sequence they are typically very active, having a strong magnetic field and emitting frequent stellar flares. The strong magnetic field of the young star interacts with the outgoing stellar wind, forcing the wind to co-rotate at large distances, thereby causing the star to lose angular momentum and ultimately leading to a spinning-down of the star over time. This spin down due to a magnetically constrained stellar wind is called "magnetic braking" (e.g., Mestel 1968, Skumanich 1972) and it generally coincides

[1] `http://en.wikipedia.org/wiki/Star_formation` , and references therein; see also `http://ircamera.as.arizona.edu/NatSci102/NatSci102/lectures/starform.htm`

with a weakening of the star's magnetic field over time as well as a decline in surface activity (Skumanich 1972).

K stars are believed to rotate differentially, i.e., not as a rigid body. This means that star spots at different latitudes on particular stars appear to drift across the surface of the star at different rates. We can quantify this with the term $d\Omega$, which is the difference between the angular velocity of an equatorial star spot, and a spot at a higher latitude. In Reinhold (2013), Figure 15 clearly shows that $d\Omega < 0.1$ radians day^{-1} for most M and K stars. We can then define a more intuitive quantity α, the fractional differential rotation:

$$\alpha = d\Omega/\Omega = d\Omega * P/(2 * \pi) \tag{1.2}$$

where P is the rotation period of the star. For $P < 1$ day:

$$\alpha \lesssim 0.16 * d\Omega * P \simeq 0.016 * P < 0.016 \tag{1.3}$$

This indicates that any time we observe fractional frequency differences in a star with a spread or range of more than a percent or two, they likely originate from two different stars and they are not due to differential rotation. Furthermore, It has been observed that late-type stars have differential rotation rates that depend strongly on effective temperature and weakly on rotational period (Barnes et al. 2007; Reiners 2006). This dependence has also been observed in computational simulations (Küker & Rüdiger 2011, Reinhold 2013).

1.2 The *Kepler* Mission

NASA's *Kepler* satellite (see Figure 1-2) was developed to search for exoplanets, which are planets that orbit stars other than our own Sun. It was designed to achieve this goal through the use of a large mosaic of CCDs at the focus of a telescope which monitors a fixed field of view of 115 square degrees. Since *Kepler* is in space, there is no atmosphere to hinder its vision of the Milky Way stars, enabling it to detect very

low amplitude flux variations, including exoplanet transits around distant stars. It is capable of this feat due to its high photometric precision of about 20 parts per million (ppm) on a 12 magnitude star over a 6.5 hour integration. *Kepler's* photometric samples usually occur with a cadence of 29.4 minutes. Over the course of its mission, the *Kepler* satellite has monitored over 150,000 stars almost continuously for close to four years (Borucki et al. 2011; Bathalha et al. 2013). Since 2009, the *Kepler* satellite has discovered thousands of planets, as well as 2600 binary stellar systems. The immense size of the *Kepler* data set enables one to study large numbers of K stars at once. See Figure 1-2 for an image of the *Kepler* Satellite's field of view of the sky.

1.3 Thesis Content

In this thesis, it was my goal to (1): find young and still rapidly rotating K stars with rotational periods of 2 days or less, and (2): to identify *Kepler* targets with several fast rotation periods which we attribute to bound binary, triple, and possibly higher order stellar systems. I will describe my search through the *Kepler* data set of K dwarf stars for the rapidly rotating members of this class with rotation periods of 2 days or less where Fourier transforms were used to find and to identify rotation periods. I provide a tabulated list of these rapidly rotating K stars. As a special subset of these I also provide a table of some 17 targets that are interpreted as binary and hierarchical triple stellar systems containing young, rapidly rotating stars. I will argue that these 17 systems have ages on the order of hundreds of millions of years. I will provide imaging evidence for the multiplicity of 6 of these 17 stellar systems, and finally I will summarize my results and conclusions.

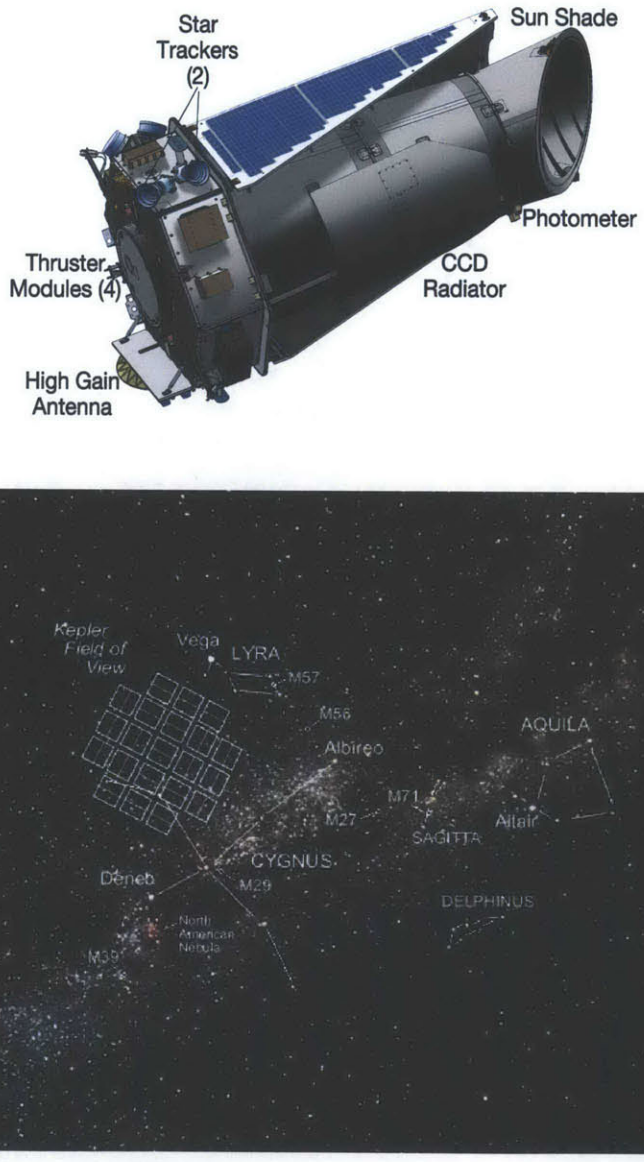

Figure 1-2 Top: A diagram depicting NASA's *Kepler* satellite. Bottom: The *Kepler* satellite's field of view is projected onto an actual image of the Milky Way as seen from Earth. The field of view is roughly centered on the direction of the constellation Cygnus (http://kepler.nasa.gov/images/MilkyWay-Kepler-cRoberts-1-full.png).

Chapter 2

Search for Rapidly Rotating K Stars

Stars of many varieties, including our own Sun, have been observed to exhibit star spots. Each of these spots can cover up to a few percent of the star's surface. The effective temperature observed for a star spot is significantly cooler compared to the rest of the stellar surface. For example, consider a star that has spots that are 15% cooler than the surrounding stellar surface. This means that $\Delta T/T_{\rm star} \sim 15\%$ where the difference in effective temperature between the starspot ($T_{\rm spot}$) and stellar ($T_{\rm star}$) surfaces is ΔT. The luminosity of a blackbody is proportional to its effective temperature to the fourth power: $L \propto T^4$. Thus, the amount of flux coming from the spot is about 50% lower than the flux coming from an equivalent area of hotter stellar surface. Suppose one of these spots is located on the host star's equator and an observer is located in the rotational plane of the star. The observer would find that this equatorial star spot causes periodic photometric light variations, i.e., the net flux reaching the observer would fluctuate in time with a period equal to the rotational period of the host star. As the spot rotates across the equator of the star, the spot would block some of the light from the star, making the star appear a little darker and allowing less flux to reach the observer. In contrast, as the spot traverses the far side of the star the net flux would appear to remain at normal levels. One can imagine that with numerous starspots at several different stellar latitudes

and longitudes, approximately sinusoidal photometric modulations in flux can readily arise from rotating star spots.

For a spot on a star located more generally, the apparent brightness of the star is altered in time t (minus the effects of limb-darkening) by such a spot according to:

$$\Delta F = \epsilon[\cos(\alpha)\cos(i) + \sin(\alpha)\sin(i)\cos(\omega t + l)] \tag{2.1}$$

where α is the colatitude of the spot on the star, l is the spot longitude, and i is the inclination of the star which is the angle between the rotation axis and the observer's line of sight (Tran et. al 2013). The constant, ϵ, quantifies the photometric strength of the spot, has units of flux, and is assumed to be much smaller than the total flux from the star. It can be estimated as:

$$\epsilon \simeq \frac{4\Delta T}{T}\frac{\pi r_{\text{spot}}^2}{\pi R_1^2}B_0 \tag{2.2}$$

where R_1 is the radius of the star, r_{spot} is the radius of the spot, ΔT is the same as above (the difference in effective temperature between the stellar and spot surfaces), and B_0 is the mean brightness of the star. Limb-darkening further complicates this picture: the edges of the star are darker than the center of the star because the observer sees less deeply into the star where the effective temperature is lower. After taking the effect of limb-darkening into account, equation (1) becomes:

$$\Delta F_{\text{spot}} = A + b(1 - u + 2au)\cos(\omega t + l) + ub^2\cos^2(\omega t + l)] \tag{2.3}$$

where $a \equiv \cos\alpha\cos i$ and $b \equiv \sin\alpha\sin i$, A is a DC offset, and u is the linear limb-darkening coefficient. See Figure 2-1 for a couple of simulated starspot modulation patterns based on equation (3) for one and two stellar spots on the surface of a star. In the top panel two simulations are plotted, one with one spot (blue curve) and one with two spots (green curve). In both simulations, one of the spots was located at $\alpha = 45°$, $i = 40°$, $l = 30°$, and $u = 0.44$. In the case of the green curve, an additional spot was added with the parameters $\alpha = 45°$, $i = 40°$, $l = 210°$, and $u = 0.44$. Furthermore,

the second spot was assigned an amplitude that was 0.3 times the amplitude of the first spot. In the bottom panel, again two spots are simulated in such as way as to produce double−peaked light variations. The parameters of these spots are the same as in the top image, except the colatitude and longitude of each spot was changed. In this case the first spot was located at $\alpha = 30°$, $l = 30°$, and the second spot was located at $\alpha = 110°$, $l = 210°$. Lastly, the second spot was given an amplitude equal to that of the first spot. The double peaked light variations arise because the second spot disappears on the far side of the star when the first spot is brightest, and then the second spot is brightest when the first spot is dimmest.

As can be seen in these simple star spot simulations (Figure 2-1), the rotation of a star with one or more spots can yield periodic photometric light variations. This phenomenon is readily observed in the *Kepler* photometric data base. For example, Figure 2-2 shows two illustrative light curves of stars with spots from the *Kepler* data set. In these light curves, photometric variations due to stellar rotation are readily seen.

The *Kepler* data have a cadence of about a half hour, or 0.0204 days, giving the spacecraft $\sim$ 50 samples per day. For rapidly rotating K stars, the shortest rotation rate that we observe it around 5 hours. This means that even for the fastest K star rotators, *Kepler* would sample at least 10 measurements per rotational period. Therefore, the *Kepler* data have the temporal resolution necessary to study photometric light variations mediated by stellar spots for even the fastest rotating K stars. *Kepler's* temporal resolution, in conjunction with its photometric precision, makes its data excellent for studying stellar rotations.

I chose to utilize Fourier transforms ('FT') in my search for spotted stars that rotate with short periods because it is a very efficient tool for finding periodic signals with a high-duty cycle and smoothly varying profiles. McQuillan et al. (2013) found that both Fourier transform and autocorrelation function (ACF) analyses were useful in their search for star spot periodicities in M dwarf targets within the *Kepler* photometric data base. Star spots are transitory in nature which can induce erratic changes in the modulation phase. Changes in the modulation phase and differential

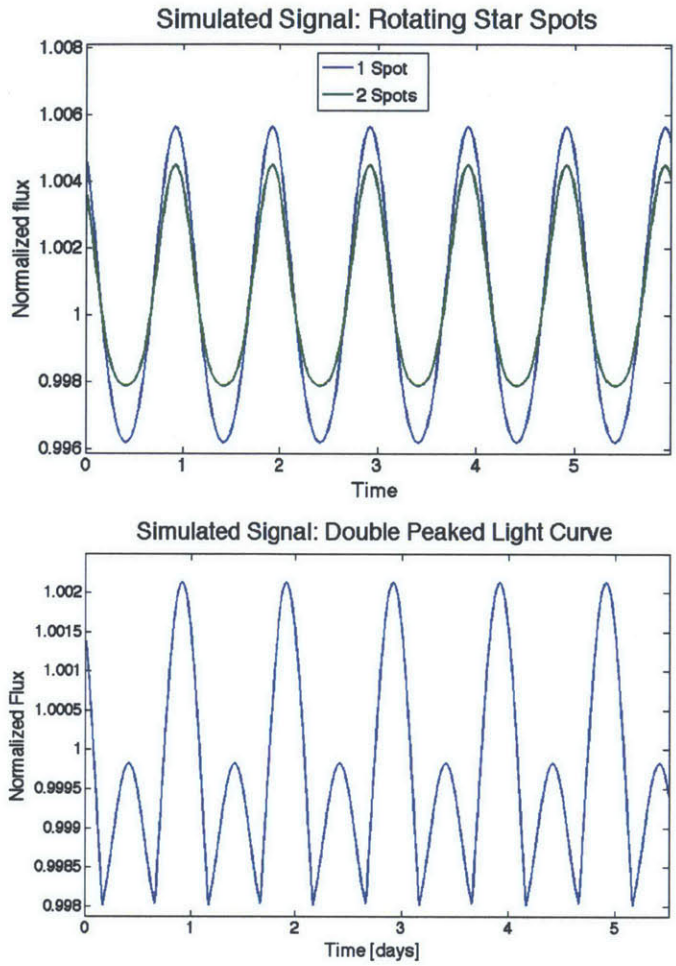

Figure 2-1 Top: A simulated light curve of a star with a single (blue curve) or two stellar spots (green curve). In both cases, the spot colatitude (α) was taken to be 45°, the inclination angle i of the observer was taken to be 40°, and the linear limb-darkening coefficient (u) is taken to be 0.44. In the case of the blue curve, a single spot with a longitude of 30° was assumed. For the green curve, an additional spot was added which had 1/3 the amplitude of the first spot. This second spot was given a longitude of 210° (180° offset from the first spot). In both cases, each spot is visible during the entire period of rotation of the star due to the observer's inclination. Bottom: Two spots are again simulated, producing a double-peak light variation. The location of the first spot is $\alpha = 30°$, $l = 30°$ and the location of the second spot is $\alpha = 110°$, $l = 210°$. The parameters i and u are the same as for the top panel.

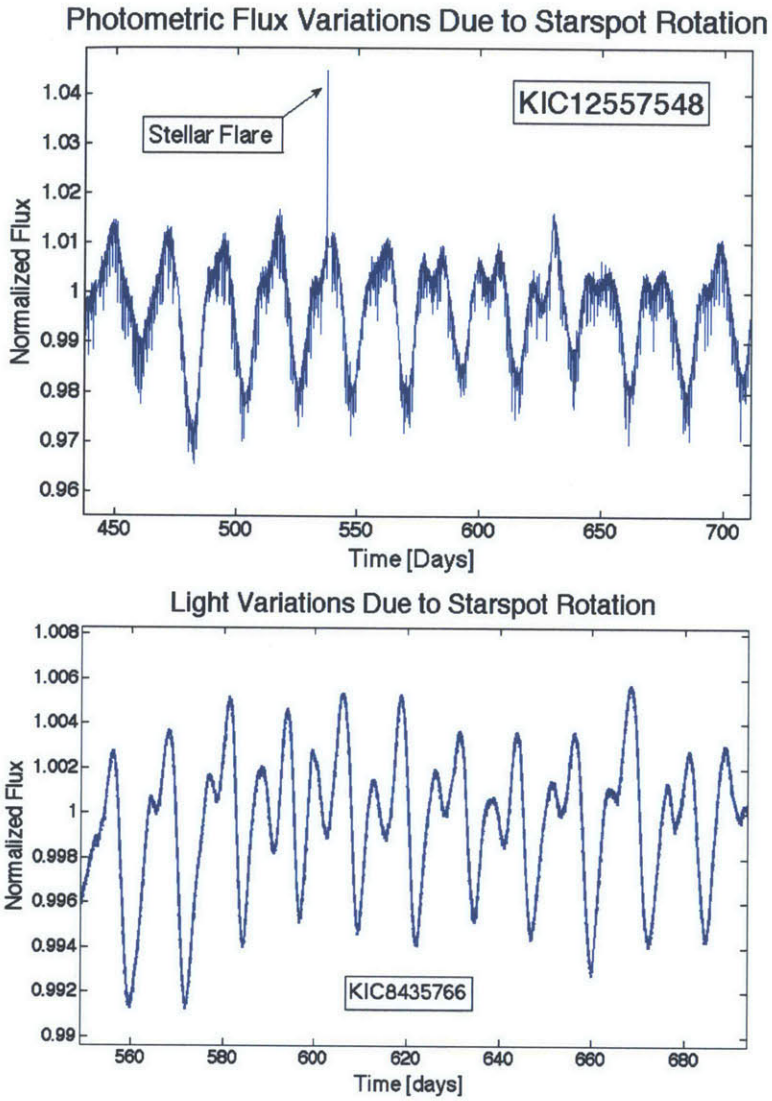

Figure 2-2 Top: Stellar flux variations in KIC12557548 due to the rotation of stellar spots every $\sim$ 23 days. The amplitude of the flux modulations is $\sim$ 4% (peak to peak). Note how the shape of the waveform changes over time: this can be due to a combination of differential rotation of the star as well as the growth or shrinking of certain spots over time. Even though this star is rotating slowly with a rotational period of $\sim$ 20 days, it is still active enough to have occasional stellar flares. The small periodic vertical dips in flux are attributed to a transiting exoplanet. Bottom: Another example of stellar flux variations due to spot rotation

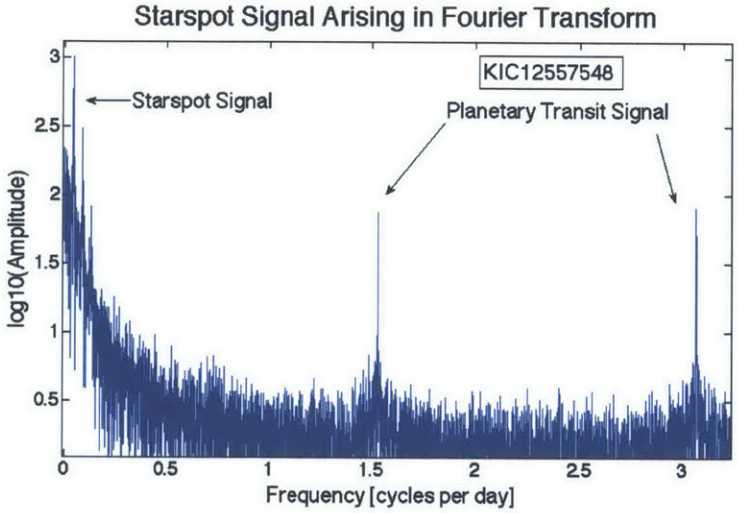

Figure 2-3 An illustrative FT of the *Kepler* target shown in Figure 2-2. A set of harmonics due to the rotation of starspots is observed as well as a set of harmonics (which continue off the plot) that belong to a transiting exoplanet.

rotation of stellar spots can broaden the peaks in a Fourier spectrum. Despite these difficulties I did not find it necessary to employ an autocorrelation function (ACF) analysis. The FTs that were produced in our analysis were clear enough for one to identify K-star targets that exhibit multiple independent periods, while it is expected that an ACF analysis would have been less straightforward in identifying multiple independent periods, especially when the differences between the periods are small.

In this work we employed an FT analysis approach that is quite similar to the one utilized in Sanchis-Ojeda et al. (2013) in their search for short-period planets as well as the one used in Rappaport et al. (2014) in their search for rapidly rotating M stars. I took the available *Kepler* PDCSAP_FLUX data (corrected with PDCMAP for various artifacts; Stumpe et al. 2012; Smith et al. 2012) which were normalized quarter-by-quarter with their quarterly median values and stitched together into a single data file. Any gaps in the data train were replaced with the mean flux value. For each star, FTs were computed and searched for peaks that represent periodic flux variations. For typical *Kepler* stars, periodic variations with amplitudes as small as a few parts per million (ppm) can be detected. Furthermore, we proceeded to

renormalize each FT by dividing by a smoothed version of the FT. These smoothed FTs were computed by convolution with a boxcar function that is 100 frequency bins in length. This renormalization process has the effect of normalizing the original FT against its local 100-bin mean, so that the significance of a peak is more easily identified.

I chose to focus on K dwarf stars which exhibit FT signals that are characteristic of star spot rotation with periods of 2 days or less. To fulfill my selection criteria, we chose to analyze all of the stars with an effective temperature between 4000 K and 5000 K, as well as having $\log g > 4$ where g is the local acceleration on the surface of the target star. This method of selection ensures that we are only focused on K dwarf stars. We then identified and gathered all target stars with renormalized FTs that possessed at least one frequency bin exceeding the local 100-bin mean by a factor > 4 with at least one additional harmonic or subharmonic that exceeded its local mean by a factor of > 3. Any stars that fit these initial search criteria were considered to be worthy of further investigation.

See Figure 2-4 for two examples of strong signals in Fourier transforms resulting from the rotation of a K star. The peak 'A1' corresponds to the base frequency of a set of harmonics that are all believed to belong to the rotation of starspots. See Figure 2-5 for a zoom in on the base frequency of KIC 39358030 (where the full FT is shown in the bottom panel of Figure 2-4). As can be seen in this transform, the Fourier peak is considerably broadened; this is likely due to differential rotation and growth and disappearance of starspots on the stellar surface.

I found that out of 14,440 K stars in the original sample, 846 met my initial search criterion. These 846 with interesting FTs were examined by eye to eliminate eclipsing binaries and known planetary systems from the list. This was done simply by checking the header of each FT, which was labelled with the words 'planet' or 'binary' if the system was a known planetary or binary system. Additionally, I checked the detected FT signal and made sure that the harmonics were monotonically decreasing (where stellar spots tend to drop off quickly, while planets and binaries tend to have a long string of higher harmonics with very slowly falling amplitudes) and I made sure that

the harmonics were not alternating in amplitude, which may be indicative of a binary system. We folded the data about the base frequency of interest and were readily able to rule out cases of transiting planets because their folded light curves have a characteristic sharp and relatively rectangular dipping profile. Furthermore, I cross-checked our list of interesting targets against the *Kepler* Objects of Interest (KOI) planet list for any matches. Lastly, all of the targets that were present in the *Kepler* eclipsing binary star catalog were eliminated from the list.

Of the aforementioned 846 initial targets that exhibit the requisite significant base frequency plus at least one significant harmonic, 293 of the targets had a base frequency of 0.5 cycles per day or higher (such as those described in Figure 2-4) and were not found to be planetary systems or eclipsing binaries. A list of these 293 systems can be found in Table 5.1. I believe that the majority of these remaining targets are rapidly rotating stars, and the signal identified in their corresponding FTs is due to star spots modulating the stellar flux as they rotate around the stellar surface. See Figure 2-4 for some typical examples of what these starspot induced signals look like after being Fourier transformed.

The list of rapidly rotating K stars was further scrutinized to find objects that exhibit multiple stellar spot rotation signals. In particular I searched for systems that exhibited multiple independent base frequencies each accompanied by higher order harmonics. Some 17 of these 293 interesting targets were found to have multiple sets of independent rapid rotational frequencies. See Figures 2-6 through 2-8 for example targets from this list of 17 systems with multiple base frequencies. In Figure 2-6 there are two targets, KIC 4819564 and KIC 5115335, where each exhibits two distinct base frequencies (A1 and B1) which are interpreted as each belonging to their own rapidly rotating star. In Figure 2-7 there are two targets, KIC 5793299 and KIC 10618471, each of which exhibit three distinct base frequencies (A1, B1, and C1) and are interpreted to be hierarchical triple systems. Similarly, the targets in Figure 2-8 also exhibit 3 independent base frequencies. These aforementioned 17 targets are all interpreted as being physically bound hierarchical binary (e.g., Figure 2-6) and triple systems (e.g., Figures 2-7 and 2-8) and are listed in Table 5.2. The histogram of all

of the rapid periods found in this study is shown in Figure 2-9.

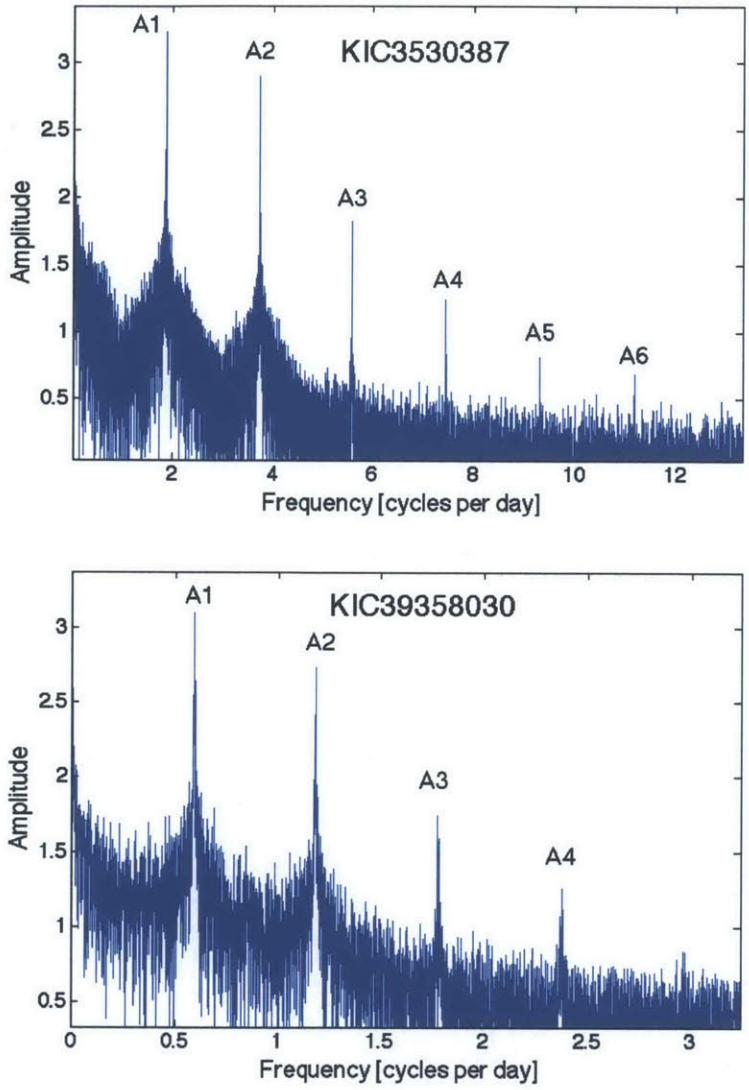

Figure 2-4 Illustrative FTs for two *Kepler* target stars: KIC 3530387 and KIC 39358030. The y-axis is a logarithmic amplitude scale to the base 10. In the text I argue that these are rapidly rotating K stars where the period of rotation is less than 2 days, which corresponds to the observed base frequency (A1). KIC 3530387 is measured to have a rotational frequency of 1.8643 cycles per day, and KIC 39358030 has a rotational frequency of 0.5941 cycles per day. These sorts of spot modulations generally have FTs with a strong base frequency (A1) as well as several higher order harmonics that are weaker in amplitude (A2 through A6). The harmonics drop off in amplitude monotonically and rapidly as would be expected from the rotation of stellar spots where the flux modulation is mostly smooth.

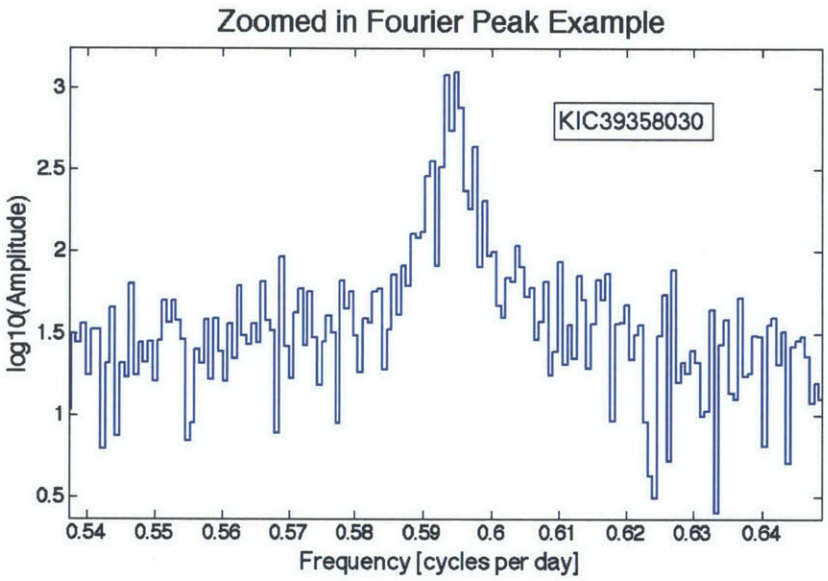

Figure 2-5 A zoom−in on the strong Fourier peak corresponding to the rotational frequency of this particular star (see also Figure 2-4). The broadened peak is likely due to differential rotation as well as the birth and disappearance of stellar spots.

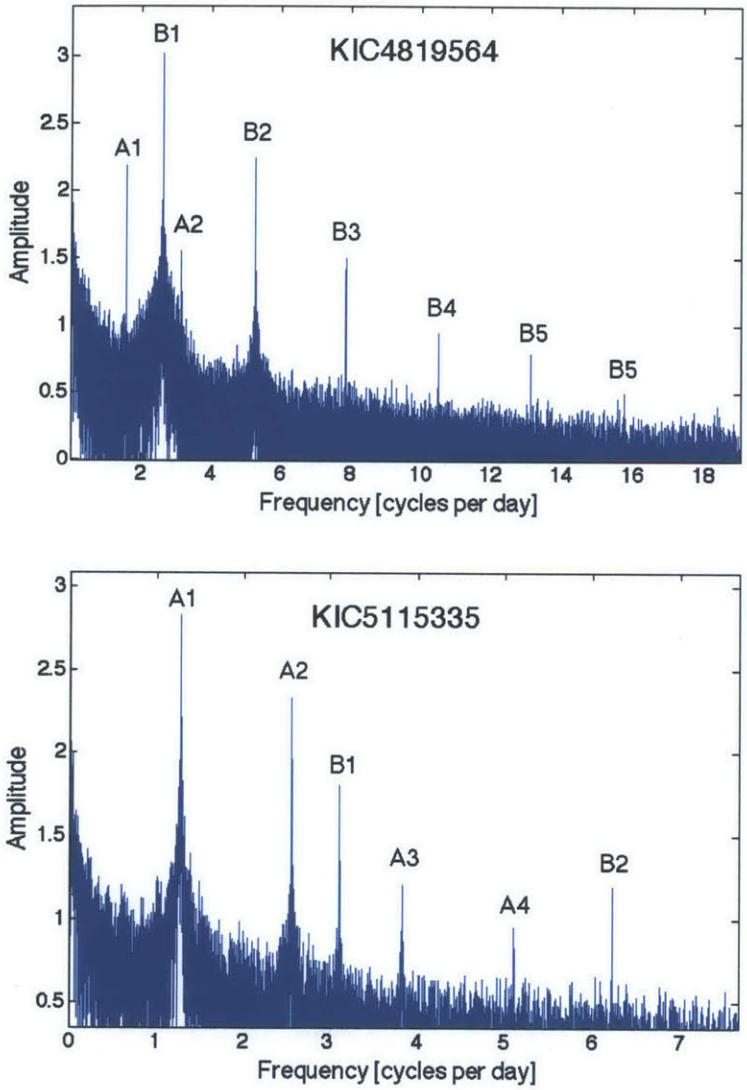

Figure 2-6 Two illustrative FTs of KIC 4819564 and KIC 5115335 which each exhibit two distinct base frequencies (A1 and B1), as well as a set of higher harmonics that correspond to their respective base frequencies. For example, the harmonics A2, A3... etc. belong to their base frequency A1. These independent base frequencies (A1 and B1) imply the existence of two rapidly rotating stars in close proximity to each other. These are interpreted to be binary systems, where both stars within the binary are rapidly rotating.

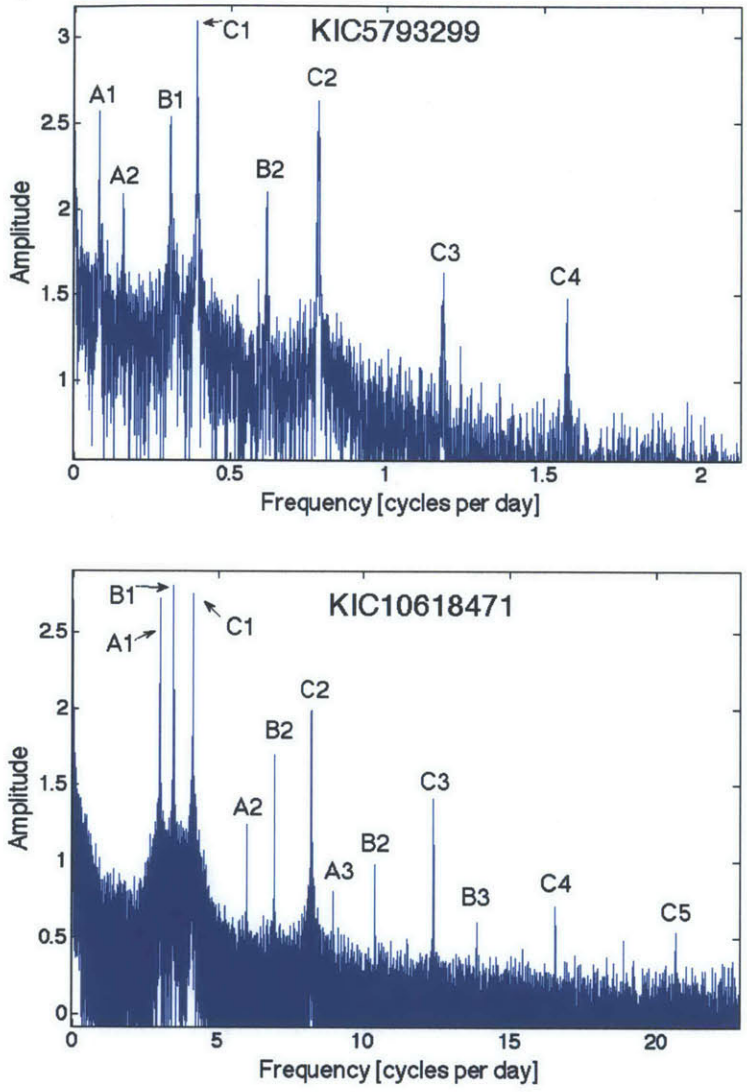

Figure 2-7 Illustrative FTs of two target stars, KIC 5793299 and KIC 10618471 which exhibit these distinct base frequencies. The 3 base frequencies are labeled (A1, B1, and C1), as well as their harmonics where, e.g., A2, A3, etc. belong to A1. These independent base frequencies (A1, B1, and C1) imply the existence of 3 rotating stars in close proximity to each other. Namely, these are interpreted to be hierarchical triple systems. In the case of KIC 5793299 (top), all three stars are rotating too slowly to be considered "rapidly" rotating, and the system was thus excluded from Table 5.2; however, since it is believed to be a triple star system, I think that it is still quite interesting and that it nonetheless deserves to be discussed. In the case of KIC 10618471 (bottom), all three stars are rapidly rotating with periods $< 1/2$ day.

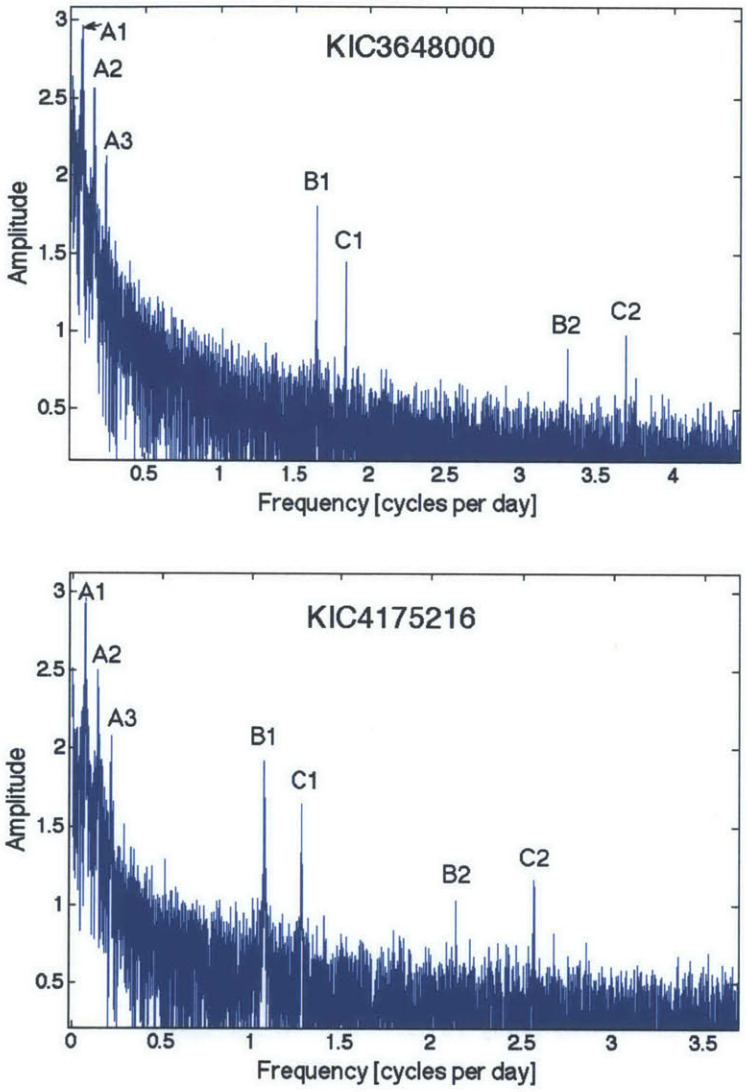

Figure 2-8 Further illustrative FTs of two target stars, KIC 3648000 and KIC 4175216 that each exhibit 3 distinct base frequencies. These are interpreted to be hierarchical triple systems. In both cases, the base frequency A1 is too slow to be considered rapidly rotating; however, the base frequencies B1 and C1 are both fast enough to be included in Table 5.2. The labeling convention is the same as in Figure 2-7.

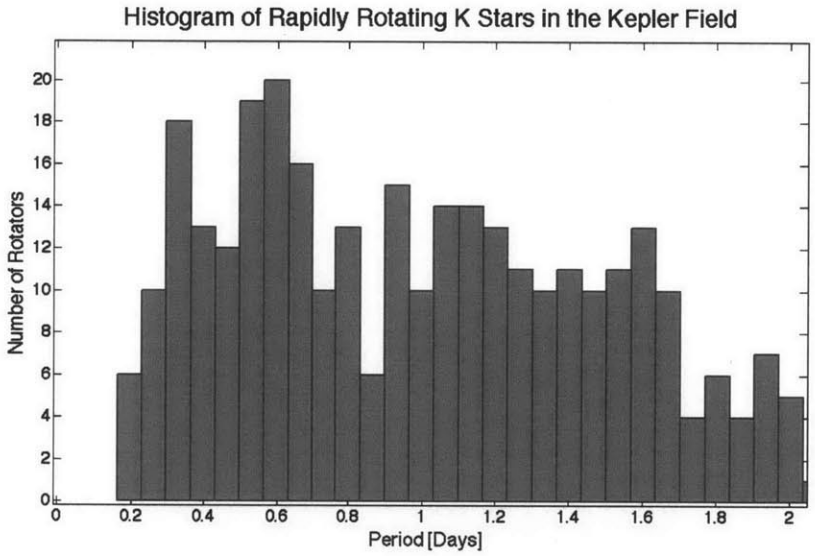

Figure 2-9 A histogram of every K star rotational period found to be less than 2 days.

Chapter 3

UKIRT Image Evidence for Hierarchical Stellar Systems

The United Kingdom Infra-Red Telescope (UKIRT) is a 3.8 meter infrared telescope located in Mauna Kea Hawaii. Images of the *Kepler* field taken with this telescope in J-band are available online for public use. Typically, these images have a spatial resolution of 0.8″ - 0.9″, and are thus useful in identifying hierarchical stellar systems with sufficiently wide separations. Instructions for obtaining these UKIRT J-band images are available on the *Kepler* science center website.

I have inspected the UKIRT J-band images for the 17 targets listed in Table 5.2 which exhibit 2 or 3 independent rapid rotation frequencies. Generally when it comes to UKIRT images within the *Kepler* field, it is possible to distinguish between two stars of similar brightness that are separated by about 1.5″ or more. However, for stars that are closer than 1″ apart, there is only a single visible stellar image. In some cases, it is possible to observe elongated stellar images for a pair of stars that are separated by as little as about 0.5″ and one can infer that the object is likely a binary. Eleven of the UKIRT J-band images of our selected targets appear to have only single, non-elongated stellar images. However, 6 of these UKIRT images show close companion stellar images and/or elongated stellar images, as seen in Figure 3-2. Generally, these companion images are within 4″ of the stellar image of the target star. Therefore, we have tentative imaging evidence for multiplicity for about 35% of

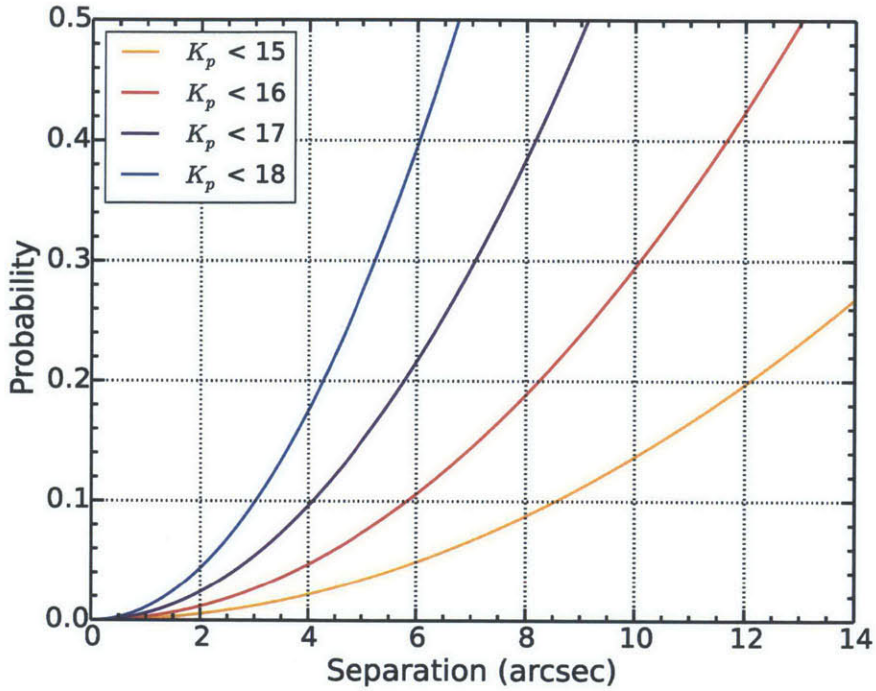

Figure 3-1 Probability of chance alignment between a foreground or background star within various angular distances from the target star (Rappaport et al. 2014) . K_P is the apparent magnitude of an apparent companion star. This demonstrates that the odds of finding a nearby companion, by chance, within 2 magnitudes of a target star that is brighter than 15th magnitude are only about 10% for a separation of 4″ and 20% at a separation of about 6″.

the systems in Table 5.2.

The *Kepler* data base provides measurements for each target star including their effective temperatures, $T_{\rm eff}$, and their apparent *Kepler* magnitude, K_p, as well as many other parameters. We want to know the approximate distances to various target stars in the *Kepler* field for the purpose of estimating the apparent physical separation of stars with a given angular separation. We can estimate the absolute magnitude of these *Kepler* stars by using data from the Rochester Spectral Classification table[1] which provides a list of stars of various spectral classes as well as the corresponding effective temperature and bolometric magnitude, $M_{\rm bol}$. For a rough approximation I selected five of these stars and plotted $\log(T_{\rm eff})$ vs $M_{\rm bol}$. A linear fit to these points

[1] `http://www.pas.rochester.edu/~emamajek/spt/`

produced the equation: $M_{bol} = 75.45 - 18.83\log(\mathrm{T_{eff}})$.The *Kepler* satellite measures light from 400-865 nm, which constitutes the *Kepler* bandpass. This is sufficiently broad that we can say the *Kepler* magnitude K_p is approximately equal to the apparent bolometric magnitude for stars with the T_{eff} that we are considering. Using this fit, I provide estimated distances to my targets with multiple independent base frequencies found in Table 5.2. These distances were calculated using the relation:

$$D = 10 * 10^{[(K_P - M_{\mathrm{bol}})/5]} \tag{3.1}$$

where D is the distance between Earth and the target star in parsecs. K_p is the apparent *Kepler* magnitude of the target star, and is listed for each object in Table 5.2.

The targets listed in Table 5.2 have an average distance of about 300 pc from Earth, meaning that 1″ of separation implies a physical separation of about 300 AU (on average). In these UKIRT images, we can only resolve stellar images that are separated by 0.5″ or more (corresponding to a physical separation of 150 AU, on average). For the sake of argument, we can say that bound stellar systems tend to have orbital separations between 0.01 AU and 20,000 AU. If we assume that binary systems are distributed uniformly in terms of the logarithms of their separations (Dhital et al. 2010), we can estimate how many systems we would expect to be able to resolve. The possible orbital separations that UKIRT imaging *cannot* resolve (from 0.01 AU to 150 AU) spans a factor of 15,000, which is $\sim 10^{4.2}$. However, UKIRT imaging can resolve orbital distances of ~150 AU up through the limit of 20,000 AU, which spans a factor of about 10^2. The ratio of these exponents provides us with the approximate percentage of binaries that we can resolve: $2/(4.2 + 2) \sim 30\%$. This implies that $\sim 30\%$ of these systems are expected to have orbital separations ≥ 150 AU and could be resolved with UKIRT images. Therefore, the UKIRT image evidence for the multiplicity of the aforementioned 35% of the targets listed in Table 5.2 is consistent with the possibility that all 17 targets are in bound hierarchical systems.

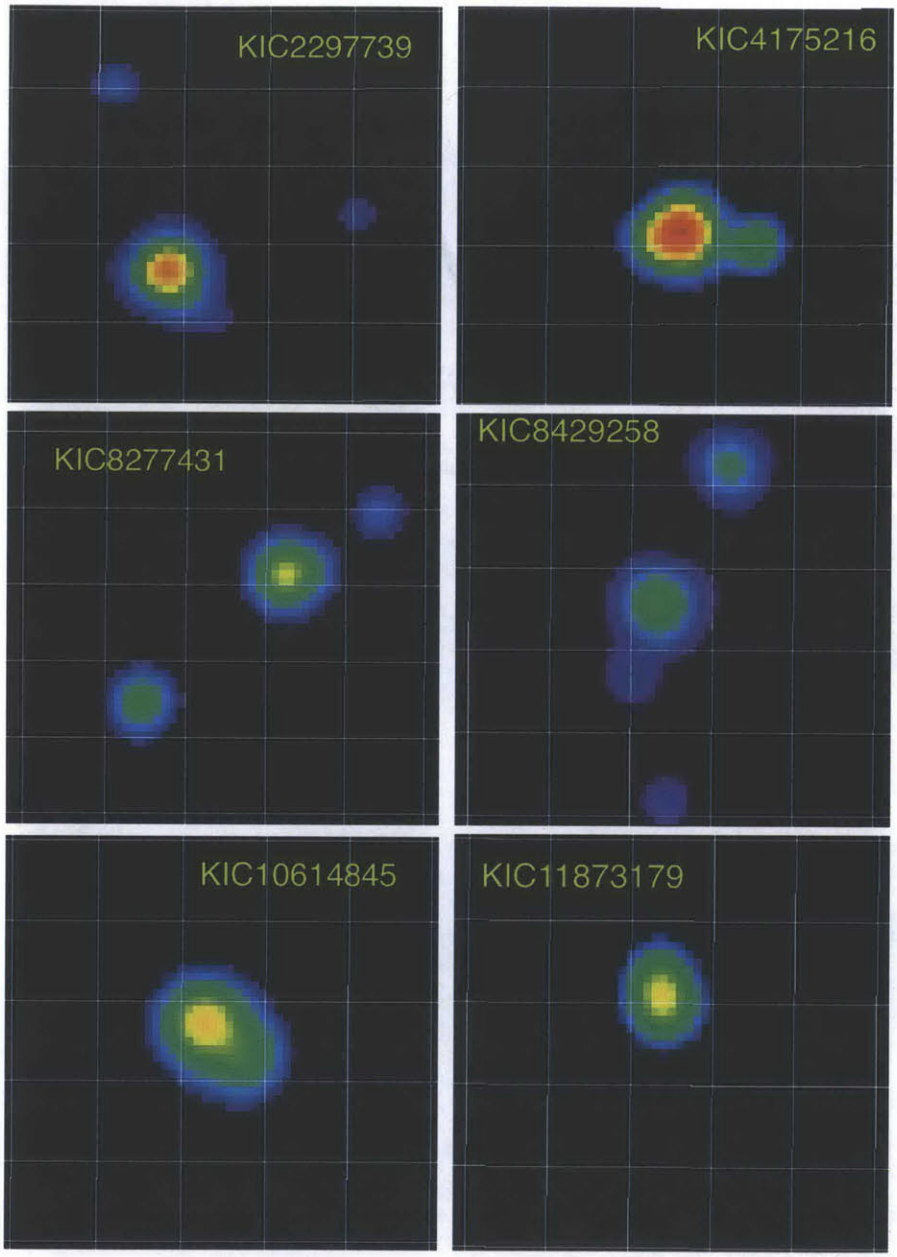

Figure 3-2 Selected set of UKIRT J-band images of *Kepler* K-stars which exhibit multiple rotation periods. The white grid lines are separated by $2'' \times 2''$. KIC 2297739 is an elongated target with two nearby fainter stars within $4''$. KIC 4175216 is sufficiently elongated to suggest that it is a double. KIC 8277431 has 2 nearby stars, one that is within $2''$ and another within $4''$. KIC 8429258 has an elongated target star image, suggesting it is a double. Furthermore, it has 2 nearby stars within $4''$. KIC 10614845 and KIC 11873179 both appear elongated, which suggests that they are both binary systems.

Chapter 4

Sonograms

Sonograms enable one to visualize how the amplitudes of different frequencies vary with time. This is a useful tool for determining if the amplitudes of periodic signals are dependent or independent of other frequencies. Thus, sonograms can be used to cross-check dependency of one frequency on another.

Dr. Katalin Oláh, a colleague of Professor Rappaport's at Konkoly Observatory in Hungary, kindly provided us with an illustrative sonogram for a particular target in Table 5.2, KIC10618471, as seen in figure 4-1 (see also Figure 2-7). This sonogram was constructed by displaying Fourier amplitudes vs frequency in the vertical direction and then plotting these strips horizontally with time. The data intervals are about 30 days for each FT, but they are stepped by only $\sim$ 2 days between FTs. Therefore, there is considerable overlap between one FT and the next. We observe that the amplitudes vary erratically and independent of what the other frequencies are doing. The erratic nature of the amplitudes of these frequencies leads us to conclude that these likely come from rotating star spots as opposed to stellar pulsations (which would be more regular). Furthermore, the relative independence of the amplitudes of the different frequencies suggests that these three frequencies all come from different stars.

We must consider the possibility that these three frequencies come from spots at different latitudes on the star and that the star is undergoing differential rotation. The frequencies in figure 4-1 differ by about 10%, indicating that:

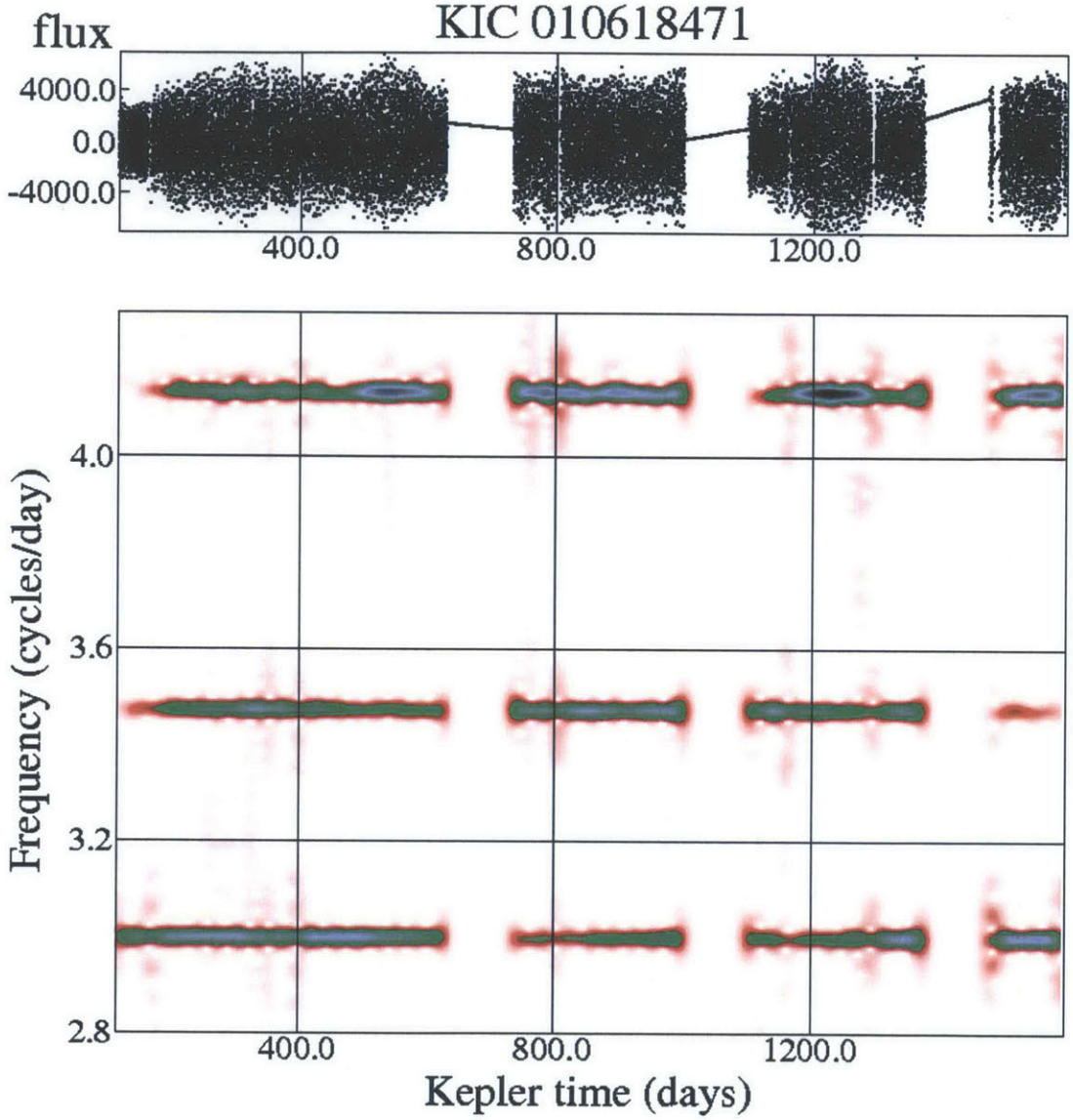

Figure 4-1 An illustrative sonogram of the target star KIC10618471, which is one of the objects listed in Table 5.2. Fourier amplitudes vs. frequency are plotted vertically, and these amplitudes are then displayed as a function of time horizontally. The three frequencies exhibit strong and erratic amplitude fluctuations with time. Furthermore, the fluctuations of the three amplitudes vary independently of each other. The erratic nature of these amplitude flucturations are indicative of star spot rotation, and the independence of these fluctuations suggests that they come from different stars.

$$\frac{d\Omega}{\Omega} \sim 0.1 \tag{4.1}$$

This implies that

$$d\Omega \simeq 0.1 * \Omega = 0.1 * 2 * \pi / P \tag{4.2}$$

where P is the rotational period of the star. In turn, this implies a value for $d\Omega$ of about 2 radians day^{-1}. This is enormously larger than any $d\Omega$ listed by Reinhold et al. (2013) in his tabulation of differential rotation. Therefore, we can safely conclude that these independent frequencies are not due to differential rotation of a single star.

Chapter 5

Results and Conclusions

Following the procedure discussed in Rappaport et al. (2013), I have searched through the *Kepler* photometric data base of K stars for rapidly rotating stars. Out of 14,440 K dwarfs, 845 systems were identified as having relevant fast periodicities, and 293 systems were found to have at least one period of $P_{\rm rot} < 2$ days (Table 5.1). Furthermore, 17 of these systems were shown to have at least two independent periods where both periods are less than two days (Table 5.2). Of these 17 systems, 8 were found to have three independent periodicities; however, only one of these has all three periods less than 2 days. There are a sufficient number of these short-period systems with multiple independent periodicities to allow us to argue that they are probably young, physically related hierarchical binary and triple systems.

While conducting this study, I found that about 2% of all K stars within the *Kepler* field are rotating with a period of 2 days or less. We can utilize standard models of contraction onto the main sequence in conjunction with the consequential spinup of a star due to conservation of its angular momentum, along with the eventual loss of angular momentum due to magnetic braking (Kawaler 1988; Chaboyer at al. 1995; Barnes & Sofia 1996; Irwin et al. 2011) to check if our K stars are expected to spend enough time rotating rapidly to allow for 2% of them to have rotational periods of 2 days or less. These models usually take the magnetic braking torque to be proportional to $\omega_{\rm rot}^3$ when $\omega_{\rm rot} < \omega_{\rm sat}$ where $\omega_{\rm rot}$ is the rotational frequency of the star that is undergoing magnetic braking, and $\omega_{\rm sat}$ is a saturation frequency. The

magnetic braking torque is taken to be proportional to $\omega_{\rm rot}\omega_{\rm sat}^2$ when $\omega_{\rm rot} \geq \omega_{\rm sat}$. In Figure 5-1, we show representative spin history plots computed by Irwin et al. (2011) where the rotational frequency of a low mass star is plotted against its age. Using the top panel (in particular, the dashed curve), we estimate that the peak rotation period of 0.3 days corresponds to an age of 100 million years. Then, after an additional 200 million years (for a total age of 300 million years), the rotational period has slowed down to 1 day. Once the star has reached an age of $\sim$ 400 million years, it will have slowed to have a rotational period of 2 days. This plot assumes a maximum age of 10^4 million years. Therefore, we can estimate the total percentage of stars that will have an rotational period of two days or less to be $\sim 400/10000 * 100\% = 4\%$. This plausibly matches our measured 2% rapidly rotating K stars.

At least 6 of the 17 stellar systems in Table 5.2 exhibit multiple stellar images within 5″ of the main target star or elongated stellar images in the J-band survey of UKIRT *Kepler*-region images, as seen in Figure 3-2. These images may represent gravitationally bound stellar systems. We have found $\sim$ 300 fast rotators. If 2% of all K dwarfs have short rotation periods then unrelated nearby stars should have a 2% chance of being rapid. Furthermore the probability of finding a close ($< 6''$) neighbor with $|\Delta J| < 2$ is $\sim$ 20%. Putting these together, we expect $20\% * 2\%$ of the 293 targets to have a rapidly rotating companion at random, i.e. about one such coincidence. Since we find 6 such systems we conclude that these are related objects.

While the UKIRT images have proven useful for a quick inspection, better resolution images of these systems are needed to determine which targets are indeed hierarchical systems. The UKIRT images can only resolve stars that have angular separations of the order of 0.5″ or more. However, for a star system at about 300 pc (like that of the average target in Table 5.2), an angular separation of about 0.5″ is equivalent to a physical separation of about 150 AU. Assuming a maximum orbital separation of 20,000 AU, we deduced that about 30% of all binaries 300 pc from Earth should be resolvable in the UKIRT images. This estimated 30% matches our findings of $\sim$ 35%. If we can further reduce the detectable separations by a factor of 10 with adaptive optics imaging, we can gain another decade (out of $\sim$ 6 total) in

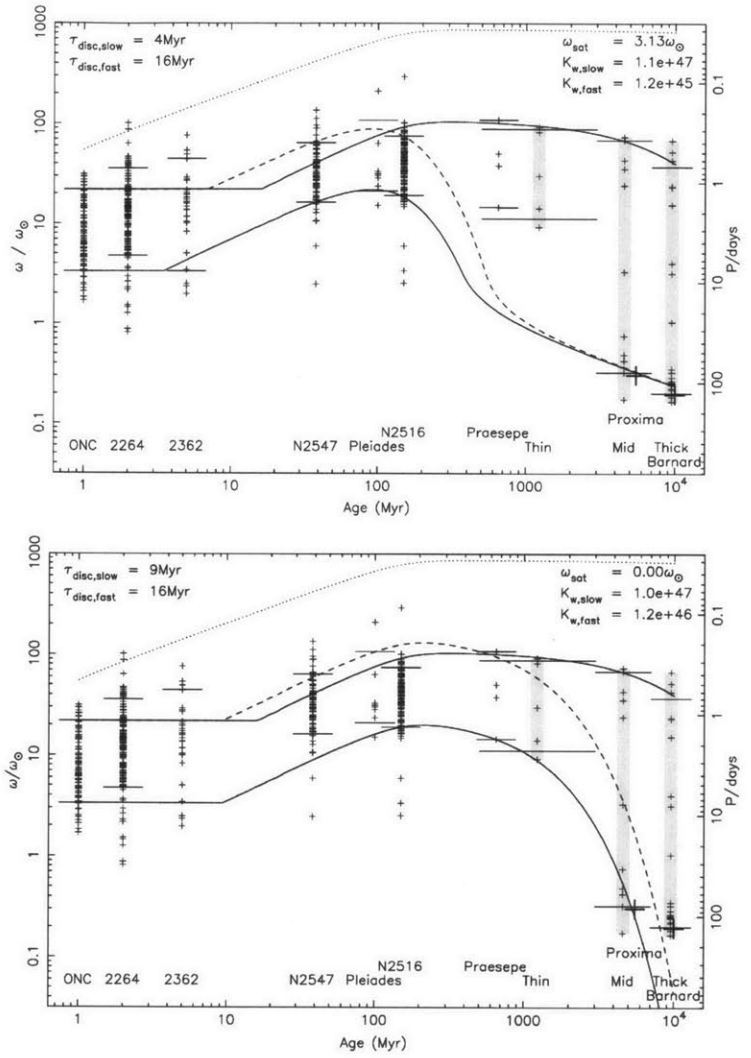

Figure 5-1 Top: An illustrative plot showing model calculations for how low−mass stars ($0.1 < M/M_\odot < 0.35$) spin up during the contraction phase of the star onto the main sequence, and then consequentially spin down due to magnetic braking over time (Irwin et al. 2011). If we focus on the dashed curve, which corresponds to rapid rotators when the stellar wind parameter is assumed to be the same as for the slow rotators rather than allowing it to vary, we see that a minimum rotational period of about 0.3 days is reached at an age of 100 million years. Furthermore, this curve predicts that spin down will then occur, resulting in a rotational period of 2 days at an age of 400 million years. The oldest age plotted on this diagram is about 10 billion years. Thus, these stars should spend about 4% of their lifetimes rapidly rotating. Bottom: A similar diagram to the top panel, except this one assumes all objects remain in the saturated regime throughout their lifetime.

separation. This should reveal another $\sim$ 15% of detectable multiples. This implies that in order to resolve hierarchical stellar systems 300 pc away where the stars have orbital separations of about 150 AU or less, one would need better angular resolution than UKIRT images can provide.

As seen in Figure 5-2, Keck adaptive optics (AO) images of candidate multiple M-star systems reveal binary (or higher multiple) stellar systems wit separations of only a few tenths of an arc second. These (top) images were taken at the Keck Observatory and are courtesy of Dr. Jonathan Swift (see Rappaport et al. 2014 for details). Both of these AO images are of *Kepler* M stars that exhibited multiple rapid rotation periods - exactly analogous to the problem that I have addressed in this thesis regarding K dwarfs. The AO images are compared to their UKIRT counterparts (bottom). While the UKIRT images could not come close to resolving these stellar systems, the Keck AO images were able to resolve them easily. Therefore, additional future adaptive optics imaging could well reveal that more of my 17 multiple-period K dwarf systems also contain two or more bound stars. Furthermore, doppler spectroscopy measurements of all 17 systems could further expose even closer gravitationally bound stars, where the angular separation is too small for adaptive optics imaging to resolve.

Thus, in this work we have found some 293 K stars that are rapidly rotating, and 17 of these targets are very likely to be young binary or triple star systems. This appears to be a very useful way of searching for young multiply bound star systems.

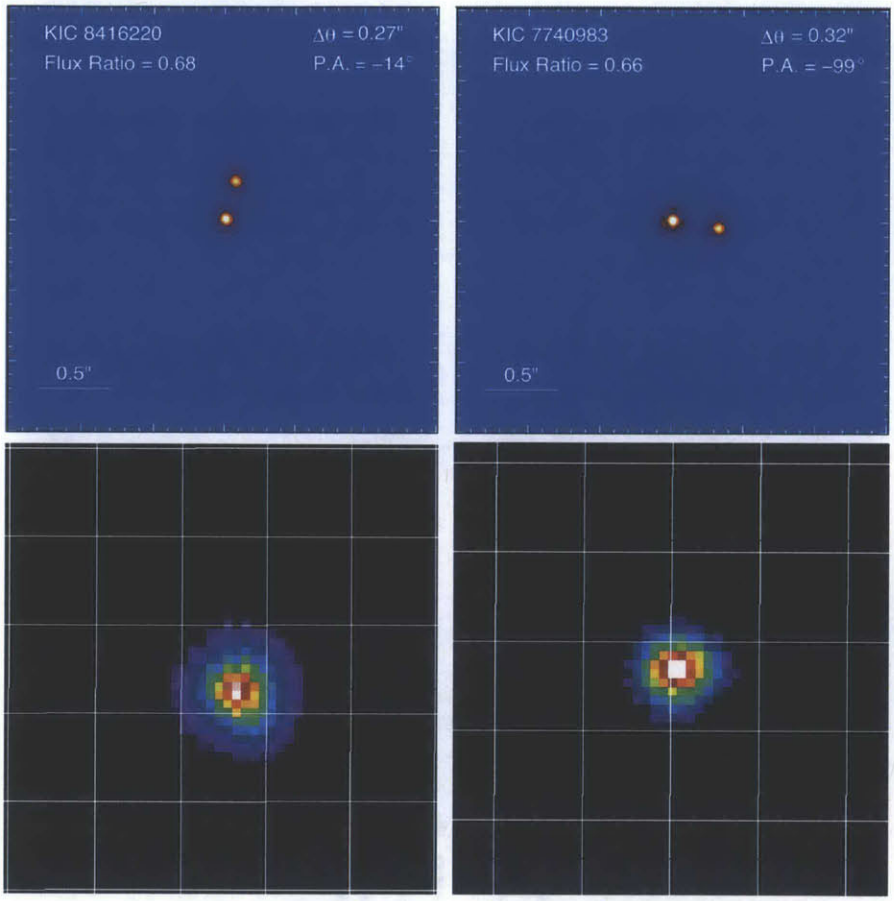

Figure 5-2 Top: Illustrative adaptive optics (AO) images for two *Kepler* M star targets, KIC 8416220 and KIC 7740983 (Rappaport et al. 2014), taken at the Keck Observatory and are courtesy of Dr. Jonathan Swift. Directly beneath each target is their corresponding UKIRT image with 2″ grid line spacing. These are clear examples of how AO imaging can resolve close binaries and triples while the UKIRT images cannot.

Table 5.1. *Kepler* K Stars Exhibiting a Short Rotation Period

KIC	Period	KIC	Period	KIC	Period	KIC	Period
1026474	1.5645	5097379	1.4184	7023973	0.3864	9850966	1.9814
1570924	0.5701	5097419	0.6436	7138162	2.0113	9851943	1.0820
2017692	0.9293	5106721	0.5768	7212025	0.2073	10002792	1.1610
2297739	1.6108	5115335	0.3211	7222939	0.7880	10004510	1.3691
2305311	0.7025	5165017	0.9748	7295373	0.7504	10063343	0.3328
2436635	1.1700	5184882	1.2497	7347292	1.3463	10081256	0.9788
2438873	0.4626	5284217	1.2375	7363684	0.7293	10136527	0.4338
2439144	1.9361	5301955	0.6842	7368999	0.9238	10161873	1.1380
2558138	1.1342	5372048	0.6652	7379583	0.4315	10162509	0.9628
2579041	1.1396	5427445	0.6434	7449976	0.9150	10165244	1.7658
2852669	1.0619	5446821	0.6471	7456455	0.5200	10226498	0.3303
2985366	0.2402	5460828	1.9164	7511885	1.2943	10231863	1.3822
3123292	0.6072	5480273	1.2770	7668857	1.5138	10263691	0.4452
3217078	1.8546	5512513	0.7754	7671053	0.5046	10276003	0.9337
3339825	0.3341	5546338	1.1269	7671841	0.6548	10290447	0.6949
3430287	0.4657	5547144	0.2648	7732556	0.3069	10293980	1.0625
3529497	1.0467	5557240	1.8660	7765236	1.7416	10320278	0.8063
3530387	0.5364	5557875	0.4666	7810798	0.4111	10355809	1.5249
3539331	1.5366	5607145	0.9819	7836762	0.8110	10453357	1.0510
3541346	0.9096	5641252	1.3848	7886049	1.4975	10464111	1.0826
3550411	1.4959	5648400	1.9249	7957709	0.6484	10515995	0.7465
3556533	1.2549	5653075	0.3297	7957881	1.0434	10583089	1.4491
3648000	0.5424	5682476	0.7695	7958890	1.6975	10614845	0.5740
3659186	1.1813	5685714	0.5129	8095028	0.3638	10618471	0.2419
3759394	1.0012	5689996	1.2140	8099615	0.9499	10684456	1.6116
3765482	0.2082	5693926	0.5708	8188059	1.5696	10712311	1.4399
3858086	1.4201	5696518	0.9637	8197767	1.2473	10732223	0.9309
3868474	0.2082	5702405	0.5445	8226542	0.9871	10918016	1.0412
3935803	1.6832	5709889	1.0537	8257779	1.4443	10935928	0.9132
3953970	1.6049	5725846	1.1745	8262490	1.0457	10991555	1.0861
3954961	1.0449	5731359	0.3508	8277431	0.3029	11017466	1.3699
3971772	1.5399	5770769	1.2151	8278323	0.9454	11080489	1.0142
4036018	1.5818	5772419	1.3556	8283996	1.0881	11087095	0.7788
4036050	1.5803	5786382	0.4029	8314902	0.8146	11087527	0.4112
4042417	0.6229	5906714	1.1322	8329506	0.2784	11133900	1.3951
4047410	0.5012	5944041	1.0976	8378945	0.6675	11186618	0.6283
4065705	1.3665	5956051	0.4467	8410368	0.9117	11193279	1.9818
4066245	1.9391	5960718	1.9402	8423343	1.7170	11196403	1.3885
4070633	0.4176	5975314	1.3326	8429258	1.1613	11240908	1.1455
4136317	1.5823	5983410	1.9666	8489855	1.1111	11241294	0.2972
4136435	1.5815	6021786	0.5529	8604020	1.5946	11245425	0.6388
4169930	0.4070	6023956	0.4246	8767669	1.0275	11299675	1.1127
4174234	0.5049	6032448	1.2267	8781283	0.4036	11342189	1.3339
4175216	0.7794	6035535	0.5733	8784119	0.4858	11350350	1.7879
4181749	1.3641	6045511	0.2736	8811811	1.5446	11393217	0.6550
4254871	1.2757	6050154	0.5667	8817358	1.2932	11403751	0.2009
4283417	0.9982	6146239	1.1912	8843859	1.5380	11453264	1.9889
4351367	1.2687	6263661	1.6779	8977179	1.5969	11495989	1.3289
4351414	0.5182	6268387	1.6521	9019191	0.7660	11509272	0.3170
4373708	0.4624	6290974	1.8769	9029375	1.7870	11521137	1.4901
4390744	0.3625	6302523	0.2766	9042516	1.0015	11617578	0.5234

Table 5.1 (cont'd)

KIC	Period	KIC	Period	KIC	Period	KIC	Period
4454890	0.8702	6342263	0.9816	9053655	0.7991	11665620	0.3628
4550909	0.7146	6343818	0.3240	9077192	1.1505	11713701	1.6779
4636938	0.4775	6344281	0.5198	9114508	1.6943	11717716	0.5113
4637562	0.6324	6344375	0.6254	9117123	0.5216	11758356	1.6941
4660038	1.5090	6347423	1.6252	9119108	0.6428	11768443	1.1173
4671547	0.8382	6363542	0.5665	9141761	0.7704	11854061	1.6861
4672010	0.4815	6423857	1.1980	9153823	1.4409	11854431	0.3195
4673107	1.4562	6445537	1.6567	9273730	0.8904	11869252	1.9175
4725292	1.1549	6542256	0.1622	9284819	1.6926	11873091	1.4584
4771930	0.7410	6612690	0.5266	9340291	1.3524	11873179	0.7407
4819423	1.7535	6668625	1.5270	9340503	0.8523	11911230	0.5676
4819564	0.3807	6675318	0.5781	9414097	1.8783	11972872	0.2655
4846603	1.9928	6752730	1.2127	9456920	1.7746	12102905	0.5750
4907159	1.5790	6753253	0.9038	9468966	1.3002	12121936	0.8692
4916039	0.4988	6762923	0.5327	9594066	0.4642	12164740	0.9027
4929092	0.5781	6774679	1.4749	9594184	0.1945	12353501	0.3117
4953211	1.3600	6863987	1.5110	9602189	1.3848	12365015	0.5961
4990413	1.8288	6871390	0.5554	9606349	0.7381	12405531	1.2302
5018976	0.7699	6880588	0.3918	9649447	1.3716	12601939	0.8880
5032343	0.5325	6924050	1.2736	9715709	0.5729	12835007	0.6086
5042629	0.2719	6947767	0.7115	9775961	1.3301	0	0.0000
5077772	0.5908	6953069	0.2940	9836233	0.7472	0	0.0000
5084199	1.5823	6967296	1.2048	9836422	1.3974	0	0.0000

Note. — 293 *Kepler* targets exhibiting at least one starspot rotation period shorter than 2 days. If more than one period is present, only the shortest period is listed here. Periods are in days. For systems with more than one short rotation period see Table 5.2

Table 5.2. *Kepler* K Stars Exhibiting Two or More Short Rotation Periods

Object (1)	α_{J2000} (2)	δ_{J2000} (3)	K_p (4)	$T_{\rm eff}$ (5)	Freq$_A$ (6)	Freq$_B$ (7)	Freq$_C$ (8)	M_{bol} (9)	Dist. (10)	Imaging (11)
3648000	19h 28m 13.68s	38d 45m 13.07s	13.565	4168	1.8438	1.6512	0.0785*	7.18	189	...
4175216	19h 42m 25.47s	39d 12m 35.68s	13.824	4262	1.2830	1.0687	0.0719	7.04	227	Elong.
4819564	19h 05m 25.31s	39d 55m 05.38s	14.672	4125	2.6266	1.5796	...	7.25	305	...
5018976	19h 36m 09.06s	40d 10m 46.52s	14.282	4322	1.2989	0.5528	...	6.94	294	...
5115335	19h 43m 30.41s	40d 12m 55.66s	14.113	4211	3.1145	1.2773	...	7.12	250	...
5372048	19h 38m 02.85s	40d 31m 04.51s	14.523	4267	1.5032	0.1728*	...	7.03	315	...
5696518	19h 15m 42.98s	40d 55m 03.43s	14.002	4449	1.0377	0.8428	0.0981*	6.75	282	...
5786382	19h 21m 16.61s	41d 02m 19.14s	13.649	4790	2.4819	0.6569	...	6.26	300	...
6871390	19h 36m 53.64s	42d 22m 47.89s	14.952	3920	1.8006	1.5320	...	7.59	297	...
8095028	19h 23m 32.65s	43d 58m 12.47s	12.070	4464	2.7484	2.5186	...	6.73	117	...
8277431	18h 44m 19.64s	44d 17m 47.36s	15.394	4321	3.3012	3.1668	...	6.94	491	Multiple
8429258	19h 24m 59.43s	44d 29m 58.34s	15.983	4670	0.8611	0.8272	...	6.43	814	Elong. & multiple
10614845	19h 48m 40.41s	47d 49m 16.07s	14.028	4802	1.7423	0.9052	0.1328*	6.24	361	Elong.
10618471	19h 52m 45.24s	47d 52m 31.67s	12.496	4788	4.1338	3.4714	2.9969	6.26	175	...
11186618	19h 18m 58.50s	48d 53m 24.29s	14.583	4569	1.5916	1.5153	0.1080*	6.57	400	Elong.
11241294	19h 21m 10.25s	48d 57m 04.57s	14.619	4185	3.3647	2.4873	0.0740*	7.20	305	...
12353501	19h 17m 48.23s	51d 10m 27.80s	12.000	4692	3.2080	2.9375	0.0756*	6.40	132	...

Note. — Above are all of the stellar systems found to have at least 2 base frequencies which correspond to rotational periods of 2 days or less. Note: * = Rotational frequency is too slow to be considered rapidly rotating, but it is still listed for reference; (1) KIC ID, (2) Right Ascension, (3) Declination, (4) *Kepler* magnitude, K_p, (5) composite $T_{\rm eff}$, (6)–(8) rotation frequency in cycles per day, (9) Calculated 'M_{bol}' using the fitting formula from Chapter 3, (10) Estimated distance to *Kepler* target in parsecs, (11) Comments on the stellar neighbors inferred from the UKIRT J-band images

Bibliography

Baraffe, I., Chabrier, G., Allard, F., & Hauschildt, P.H. 2002, A&A, 382, 563

Barnes, S., & Sofia, S. 1996, ApJ, 462, 746

Barnes, S.A. 2007, ApJ, 669, 1167

Batalha, N.M., Rowe, J.F., Bryson, S.T., et al. 2013, ApJS, 204, 24

Borucki, W.J., Koch, D.G., Basri, G. 2011, ApJ, 736, 19

Chaboyer, B., Demarque, P., & Pinsonneault, M. H. 1995, ApJ, 441, 865

Dhital, S., West, A.A., Stassun, K.G., & Bochanski, J.J. 2010, AJ, 139, 2566

Irwin, J., Berta, Z.K., Burke, C.J., Charbonneau, D., Nutzman, P., West, A.A., & Falco, E.E. 2011, ApJ, 727, 56

Kawaler, S. D. 1998, ApJ, 333, 236

Klessen, R.S. 2011, arXiv:1109.0467

Küker, M, & Rüdiger, G. 2011, AN, 332, 933

McQuillan, A., Aigrain, S., & Mazeh, T. 2013, MNRAS, 432, 1203

Mestel, L. 1968, MNRAS, 138, 359.

Rappaport, S., Swift, J., Levine, A., Joss, M., et al. 2014, ApJ, in press (arXiv: 1405.1493)

Reiners, A. 2006, A&A, 446, 267

Reinhold, T., Reiners, A., & Basri, G. 2013, A&A, 560, 4

Sanchis-Ojeda, R., Rappaport, S., Winn, J.N., Levine, A., Kotson, M.C., Latham, D. & Buchhave, L. A. 2013, ApJ, 774, 54

Skumanich, A. 1972, Ap.J., 171, 565

Smith, J. C., Stumpe, M. C., Van Cleve, J. E., et al. 2012, PASP, 124, 1000

Stumpe, M. C., Smith, J. C., Van Cleve, J. E., et al. 2012, PASP, 124, 985

Tran, K., Levine, A., Rappaport, S., Borkovits, T., Csizmadia, Sz., & Kalomeni, B.

2013, ApJ, 774, 81